Optical injection locking of monolithically integrated photonic source for generation of high purity signals above 100 GHz

Katarzyna Balakier,[1,*] Martyn J. Fice,[1] Frederic van Dijk,[2] Gael Kervella,[2] Guillermo Carpintero,[3] Alwyn J. Seeds,[1] and Cyril C. Renaud[1]

[1]Department of Electronic and Electrical Engineering, University College London, London, WC1E 7JE, UK
[2]III-V Lab, a joint Laboratory of "Alcatel Lucent Bell Labs", "Thales Research & Technology" and "CEA-LETI", Palaiseau, France
[3]Universidad Carlos III de Madrid, Av. de la Universidad, 30. Leganés 28911 Madrid, Spain
[*]k.balakier@ucl.ac.uk

Abstract: A monolithically integrated photonic source for tuneable mm-wave signal generation has been fabricated. The source consists of 14 active components, i.e. semiconductor lasers, amplifiers and photodetectors, all integrated on a 3 mm^2 InP chip. Heterodyne signals in the range between 85 GHz and 120 GHz with up to -10 dBm output power have been successfully generated. By optically injection locking the integrated lasers to an external optical comb source, high-spectral-purity signals at frequencies >100 GHz have been generated, with phase noise spectral density below -90 dBc/Hz being achieved at offsets from the carrier greater than 10 kHz.

OCIS codes: (000.0000) General; (000.2700) General science.

References and links

1. A. J. Seeds and K. J. Williams, "Microwave Photonics," Journal of Lightwave Technology **24**, 4628–4641 (2006).
2. D. Marpaung, C. Roeloffzen, R. Heideman, A. Leinse, S. Sales, and J. Company, "Integrated microwave photonics," Laser & Photonics Review (2012).
3. J. Capmany and D. Novak, "Microwave photonics combines two worlds," Nature Photonics 319–330 (2007).
4. R. DiFazio and P. Pietraski, "The bandwidth crunch: Can wireless technology meet the skyrocketing demand for mobile data?," Applications and Technology Conference (LISAT) (2011).
5. T. Nagatsuma, N. Kukutsu, and Y. Kado, "Photonic generation of millimeter and terahertz waves and its applications," International Conference on Applied Electromagnetics and Communications **49**, (2007).
6. A. Stöhr, S. Member, S. Babiel, P. J. Cannard, B. Charbonnier, F. Van Dijk, S. Fedderwitz, D. Moodie, L. Pavlovic, L. Ponnampalam, C. C. Renaud, D. Rogers, V. Rymanov, A. Seeds, A. G. Steffan, A. Umbach, and M. Weiß, "Millimeter-Wave Photonic Components for Broadband Wireless Systems," IEEE Transactions on Microwave Theory and Techniques **58**, 3071–3082 (2010).
7. L. A. Coldren, "Photonic Integrated Circuits for microwave photonics," IEEE International Topical Meeting on Microwave Photonics 1–4 (2010).
8. G. Carpintero, K. Balakier, Z. Yang, R. Guzman, A. Corradi, A. Jimenez, G. Kervella, M. Fice, M. Lamponi, M. Chtioui, F. van Dijk, C. Renaud, A. Wonfor, E. Bente, R. Penty, I. White, and A. Seeds, "Microwave Photonic Integrated Circuits for Millimeter-Wave Wireless Communications," Journal of Lightwave Technology **8724**, 1–1 (2014).
9. A. Hurtado, I. D. Henning, M. J. Adams, and L. F. Lester, "Dual-mode lasing in a 1310-nm quantum dot distributed feedback laser induced by single-beam optical injection," Applied Physics Letters **102**, 201117 (2013).

10. F. van Dijk, A. Accard, A. Enard, O. Drisse, D. Make, and F. Lelarge, "Monolithic dual wavelength DFB lasers for narrow linewidth heterodyne beat-note generation," International Topical Meeting on Microwave Photonics & Asia-Pacific Microwave Photonics Conference (2011).

11. X. S. Yao, "High-quality microwave signal generation by use of Brillouin scattering in optical fibers," Optics Letters **22**, 1329–1331 (1997).

12. W. Li, N. H. Zhu, and L. X. Wang, "Harmonic RF carrier generation and broadband data upconversion using stimulated Brillouin scattering," Optics Communications **284**, 3437–3439 (2011).

13. F. van Dijk, B. Charbonnier, S. Constant, a. Enard, S. Fedderwitz, S. Formont, I. F. Lealman, F. Lecoche, F. Lelarge, D. Moodie, L. Ponnampalam, C. Renaud, M. J. Robertson, a. J. Seeds, a. Stohr, and M. Weiss, "Quantum dash mode-locked lasers for millimeter wave signal generation and transmission," 2010 IEEE Photinic Society's 23rd Annual Meeting 187–188 (2010).

14. U. Gliese, T. Nielsen, M. Bruun, E. L. Christensen, K. E. Stubkjzr, S. Lindgren, and B. Broberg, "A wideband heterodyne optical phase-locked loop for generation of 3-18 GHz microwave carriers," IEEE Photonics Technology Letters **4**, 936–938 (1992).

15. S. Fukushima, C. Silva, Y. Muramoto, and A. J. Seeds, "Optoelectronic millimeter-wave synthesis using an optical frequency comb generator, optically injection locked lasers, and a unitraveling-carrier photodiode," Journal of Lightwave Technology **21**, 3043–3051 (2003).

16. S. Kobayashi and T. Kimura, "Injection locking in AlGaAs semiconductor laser," IEEE Journal of Quantum Electronics **QE-17**, (1981).

17. M. J. Fice, A. Chiuchiarelli, E. Ciaramella, and A. J. Seeds, "Homodyne Coherent Optical Receiver Using an Optical Injection Phase-Lock Loop," Jurnal of Lightwave Technoloy **29**, 1152–1164 (2011).

18. T. Okoshi, K. Kikuchi, and A. Nakayama, "Novel method for high resolution measurement of laser output spectrum," Electronics Letters **16**, 630–631 (1980).

19. E. Rouvalis, M. Chtioui, F. van Dijk, F. Lelarge, M. J. Fice, C. C. Renaud, G. Carpintero, and a J. Seeds, "170 GHz Uni-Traveling Carrier Photodiodes for InP-based photonic integrated circuits.," Optics express **20**, 20090–5 (2012).

20. B. Cai, D. Wake, and A. Seeds, "Microwave frequency synthesis using injection locked laser comb line selection," LEOS Summer Topical Meeting 3–4 (1995).

21. J. Esterline, "Oscillator Phase Noise: Theory vs. Practicality," Microwave Journal 72–86 (2008).

22. R. T. Ramos, P. Gallion, D. Erasme, A. J. Seeds, and A. Bordonalli, "Optical injection locking and phase-lock loop combined systems.," Optics letters **19**, 4–6 (1994).

1. Introduction

The generation and processing of signals in the microwave, mm-wave and THz frequency ranges based on photonic solutions has been under extensive investigation [1] [2] [3]. This is driven by the numerous advantages that photonics can offer, as compared with electronics-based solutions, as well as by increasing interest in high frequency generation caused by the anticipated spectrum crunch [4]. Many of the emerging application areas will require high-speed modulation, tuneability, smaller footprints and lower power consumption. All these requirements could be satisfied by integrated photonic solutions, considering that so far discrete photonic-enabled systems have proven capable of generating mm-waves through heterodyning for frequencies up to several THz [5]. Integrated photonic circuits also demonstrated the ability to generate microwave and mm-wave signals [6] [7] [8]. Previously reported approaches include two discrete free running lasers, dual mode lasers emitting simultaneously at two different wavelengths [9] [10], Brillouin optoelectronic oscillator [11] [12] and mode-locked lasers [13]. Unlike the solution presented in this paper, each of the above methods requires an external optical-to-electrical converter (photodiode or photoconductor) and thus are still limited by fibre coupling losses and polarisation dependence. A monolithic solution for the heterodyne source therefore becomes attractive in term of power consumption and control as these losses could be minimised. A considerable reduction in size is also an advantage.

The main drawback of using semiconductor lasers to synthesise higher frequency signals is that the linewidth of each laser (which is typically in the MHz range) contributes to the linewidth of the heterodyne signal. To overcome this problem there are several phase-locking techniques, such as optical phase lock loop [14], optical injection locking (OIL) [15] [16], or optical injection phase lock loop [17], which could be applied. Laser phase-locking allows the frequency of the synthesised signal to be precisely set and maintained. Moreover, reduction of the phase noise spectral density increases the potential of the source to be applied in high-data-rate wireless communication, where complex modulation formats with their attendant need for narrow linewidth carriers, such as quadrature amplitude modulation, are needed.

In this paper, we report the generation of mm-wave signals using semiconductor lasers monolithically integrated with a broad bandwidth photodiode on a single InP chip. The generated heterodyne can be continuously tuned across more than 40 GHz around the 100 GHz centre frequency. A high-spectral-purity signal with single sideband phase noise level below -90 dBc/Hz at offsets from the carrier greater than 10 kHz was experimentally demonstrated. This was achieved by phase locking both DFB lasers through optical injection locking techniques to an externally generated optical comb used as a reference.

2. Monolithic photonic integrate circuit

The photonic integrated circuit (PIC), shown in Fig. 1, has been realised on an InP semi insulating substrate. Fabrication required three stages of epitaxial growth and lithography, followed by wafer thinning, back metal deposition and cleaving to the chip size of 4.4 mm x 0.7 mm. The PIC includes active components such as two distributed feedback (DFB) lasers, eight semiconductor optical amplifiers (SOA), two electro-absorption modulators (EAM) and two uni-travelling carrier photodiodes (UTC-PD) for the optical-to-electrical signal conversion. Each of the photodiodes is coupled with a coplanar waveguide (CPW), positioned on the right edge of the PIC in such a way as to facilitate the use of a ground-signal-ground probe to extract the mm-wave signals. Passive structures such as multimode interference (MMI) couplers/splitters and optical waveguides were integrated using a butt-joint process. The PIC also has an optical waveguide output, situated at the left edge of the chip, allowing monitoring of the laser output and light injection into the chip for optical injection locking.

The two DFB lasers are 1.1 mm long. The lower laser (DFB2), as seen in Fig. 1, has a single active section that contains InGaAsP quantum-well layers situated below a grating layer with a phase shift introduced into the lasers cavity to ensure single mode operation. The upper laser (DFB1) has an 100 μm long passive phase section (PS) introduced between two separately driven active sections.

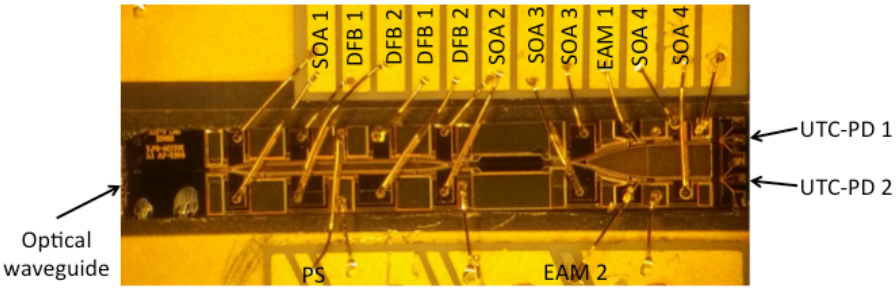

Fig. 1. Photograph of the PIC, showing notation used to describe the various elements of the device.

The DFB1 laser can be tuned through the current injection into the PS. The current tuning sensitivity was measured to be -1.45 GHz/mA, for a fixed gain current of 72 mA and for changing the phase section current between 4 mA and 20 mA. The DFB2 laser has a single gain section and has a measured tuning sensitivity of -0.37 GHz/mA.

The linewidth was evaluated separately for each laser using the self-heterodyne technique [18] with a 5 km fibre delay line, the results of which are presented in Fig. 2 a) and b), respectively for the laser with and without a passive phase section. The laser linewidth is half of the linewidth of electrical tone and the corresponding Lorentzian fits. Therefore, the FWHM optical linewidth was assessed to be about 2 MHz for the single-electrode DFB2 laser and about 3 MHz for the DFB1 laser with PS for tuning.

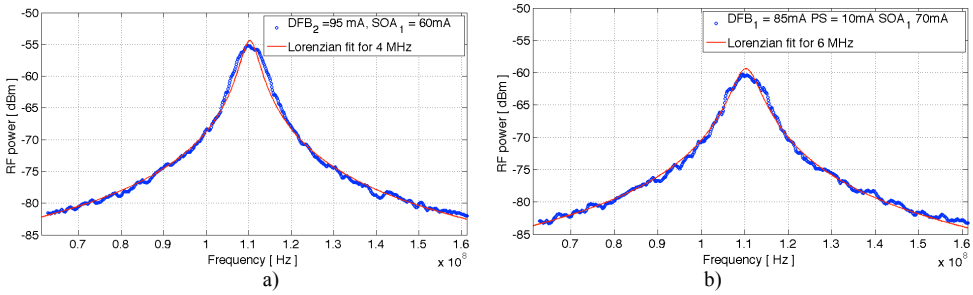

Fig. 2. Linewidth measurement of DFB lasers; Lorentzian fit gives FWHM linewidth of ~2 MHz and ~3 MHz (RBW=2 MHz, VBW=5 kHz).

The high bandwidth UTC-PD generates -0.8uA of dark current at -2.5 V bias. Similar devices fabricated previously using identical fabrication process offered an extremely high -3-dB bandwidth of up to 170 GHz [19].

Using the experimental assembly shown in Fig. 5, we can demonstrate generation of single line heterodyne signals at any frequency between 85 GHz and 120 GHz, though an even broader tuning frequency range was investigated in [8]. The frequency of the generated mm-wave signal is defined by the frequency difference between two lasers and can easily be changed by tuning the wavelength of each of the two lasers by adjusting the current injected into the DFB1 laser gain or phase section or by varying the current to the gain sections of the DFB2 lasers, as shown in Fig. 3a). The electrical spectra that correspond to optical lines demonstrated in Fig. 3 a) are presented in Fig. 3 b).

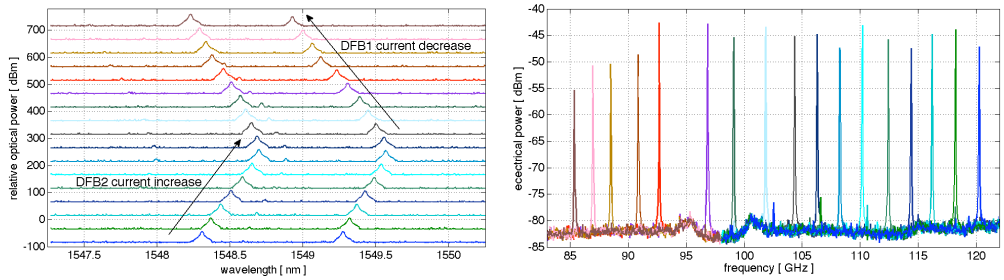

Fig. 3. Free-running optical signals generated by monolithically integrated DFB lasers (a) and heterodyne detected by integrated UTC-PD (b).

To obtain the heterodyne frequency tuning presented in Fig. 3 a) and b), the DFB1 currents were fixed I_{gain} =88mA and I_{PS} =23 mA, while DFB2 gain current was changed between 87 mA and 110 mA, allowing signals between 120 GHz and 107 GHz to be generated. Subsequently, DFB2 current was fixed I_{gain}=110 mA, while DFB1 was tuned in such a way as to generate a heterodyne between 104 GHz and 86 GHz. To avoid DFB1 operating in a multimode regime, laser-driving currents were changed between 88 mA and 60 mA for the gain current and between 22 mA and 9 mA for the PS current. Both optical and RF output of the PIC were continuously monitored. The RF power of the heterodyne signals presented in Fig. 3 b) was not corrected for losses associated with the probe, cables, sub-harmonic mixer, free space transmission, etc.

The drop in electrical power below -50 dBm for the signals below 93 GHz was mostly due to the use of WR-08 rectangular waveguides and horn antennas for probe to mixer coupling, which have an optimum operating frequency range between 90 and 140 GHz. However, a decrease in the electrical power generated by the photodiode should also be expected as a result of the reduction in optical power when DFB1 is operated at lower gain section currents.

3. Experimental arrangement for injection locking

Both DFB lasers are characterised by linewidths in the MHz range. Consequently the FWHM linewidth of the mm-wave signal should be expected to be ~ 5 MHz, however the high-frequency heterodyne signal generated at the output of integrated UTC-PD and measured on the electrical spectrum analyser exhibited FWHM linewidth of more than 10 MHz. Further linewidth deterioration was observed when additional equipment was operating in close proximity. This is thought to be due to added electrical noise being transferred onto the laser through probes and unshielded cables. To address the issue of broad linewidth of the heterodyne signal, laser phase stabilisation based on optical injection locking was implemented.

Optical injection locking (OIL) is a technique used to stabilise laser phase noise in relation to the reference source – master laser (ML). In consequence, the locked laser - slave laser (SL) follows any (within locking range) frequency excursions of an incoming optical reference. The locking is achieved by injecting part of the output light generated by a ML into the resonant cavity of the SL. The injected signal stimulates the emission inside the cavity in such a way that the SL acquires frequency and phase characteristics of the ML. This shows that OIL is an exclusively homodyne mechanism, as both SL and ML operate at exactly the same frequency [16].

To phase stabilise the mm-wave heterodyne signal using OIL, the lasers in the PIC must be locked to two optical tones derived from a common reference. In this experiment, shown schematically in Fig. 4, the reference optical source was an optical frequency comb generator (OFCG), obtained by modulating the output of a tuneable narrow linewidth (100 kHz FWHM) external cavity laser using a phase modulator with more than 30 GHz bandwidth (-3 dB). In order to obtain the required modulation index, the phase modulator was driven with 22 dBm power signal from a signal generator and RF amplifier. This resulted in an optical comb of 9 lines, with the maximum frequency spacing between the consecutive comb lines of 26 GHz (limited by the bandwidth of the high-gain RF amplifier). Using this arrangement, the highest frequency of the phase-locked mm-wave signal possible to be generated with this OFCG was limited to 104 GHz (locking to the second modulation sideband on each side of the carrier). Injection locking to the higher order side-modes was not possible because the power in these lines was too low.

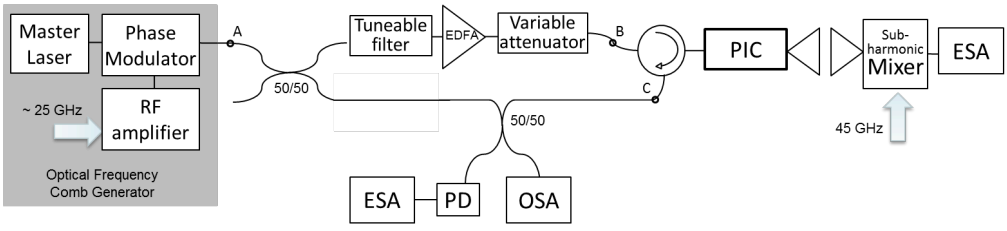

Fig. 4. Schematic representation of experimental assembly for injection locking.

A tuneable optical filter with 0.6 nm bandwidth was introduced into the optical path to supress the laser carrier and first modulation sidebands. This was done to reduce the total amount of the optical power injected into the PIC by reducing the power of the optical lines that do not serve as a reference for injection locking, but which may generate spurious outputs with the synthesised signals [20]. The reference OFCG was amplified by an external Erbium Doped

Fibre Amplifier (EDFA) to compensate for the inefficient coupling between the PIC optical waveguides and lensed fibre. Fig. 5 shows the optical spectra of the generated comb, the comb after the filter and amplifier, as well as both DFB lasers, measured at points A, B, C of Fig. 4 respectively.

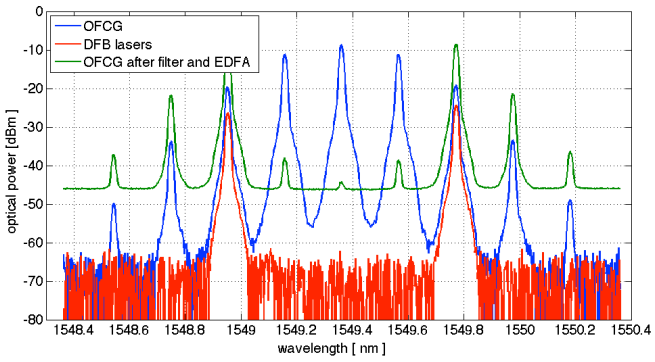

Fig. 5. Optical spectra of integrated DFB lasers and reference OFCG.

A fibre optic circulator with an isolation factor of >40 dB and a lensed fibre with a working distance of ~14 μm were used to couple light in and out the PIC. The lensed fibre gave a minimum a spot diameter of 2.5 μm, which matches the optical mode size of the ridge optical waveguide on the chip. The highest optical power measured at the output of the lensed fibre was approximately -20 dBm, while both lasers and SOA1 were operating at high current values (I_{SOA1}= 50 mA, I_{DFB1} = 85 mA, I_{DFB1_PS} = 19 mA, I_{DFB2} = 115 mA). This range of optical power is sufficient to characterise performance of both lasers, however it is lower than expected from this type of device [8], suggesting damage to the output waveguide or chip facet. It can be expected that poor coupling between the optical waveguide and lensed fibre is also affecting the amount of optical power that can be injected into the PIC and effectively into the DFB laser cavity.

The PIC optical output was also combined with the OFCG using an external fiber coupler/splitter and afterwards monitored on the high resolution optical spectra analyzer (OSA) as well as on the 40 GHz bandwidth photodiode followed by the electrical spectrum analyzer (ESA), as shown in Fig. 4.

During the course of measurements the device temperature was controlled and maintained stable at 20.5° C aided by a Peltier cooler. The heterodyne signal generated by the PIC proved resistant to temperature changes due to the fact that any change in temperature led to the change in both lasers wavelength. Therefore, the frequency difference between the lasers remained constant. The standard Peltier cooler was sufficient to control the PIC temperature and maintain the frequency of generated heterodyne signal stable for a long period of time.The mm-wave signal generated by one of the monolithically integrated UTC-PDs was extracted using a ground-signal-ground mm-wave probe with WR-8 waveguide, which was connected to a horn antenna. After a short (< 2 cm) wireless link the signal was down-converted using a sub-harmonic mixer (VDI WR8.0 SHM) to an intermediate frequency of approximately 11 GHz. The sub-harmonic mixer was driven by the LO signal of 45 GHz that was effectively doubled within the sub-harmonic mixer.

4. Optical injection locking results and discussion

The spectra of the mm-wave signal generated by the free-running and phase-locked DFB lasers monolithically integrated with a high-speed photodiode are shown in Fig. 6. A large reduction in linewidth and increase in peak power are visible when the phase stabilisation scheme is in operation.

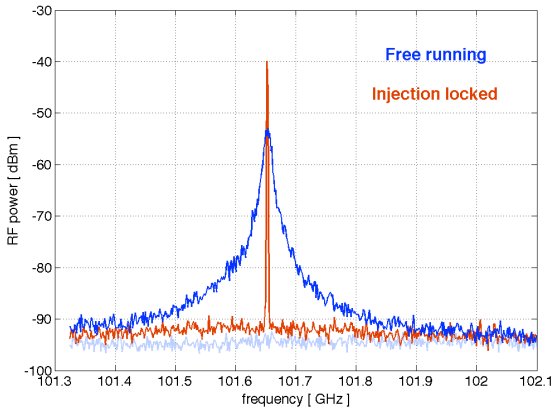

Fig 6. Electrical spectra of the free running (blue) and phase controlled (red) heterodyne signal (RBW= 300kHz, VBW = 30 kHz).

The single sideband phase noise power spectral density of the synthesised signal was measured experimentally for the heterodyne between the two DFB lasers separated by 101.7 GHz, as shown in Fig. 7. The calculated phase noise of the free running heterodyne between the two lasers, assuming summed linewidth of 5 MHz, is included in Fig. 7 for comparison.

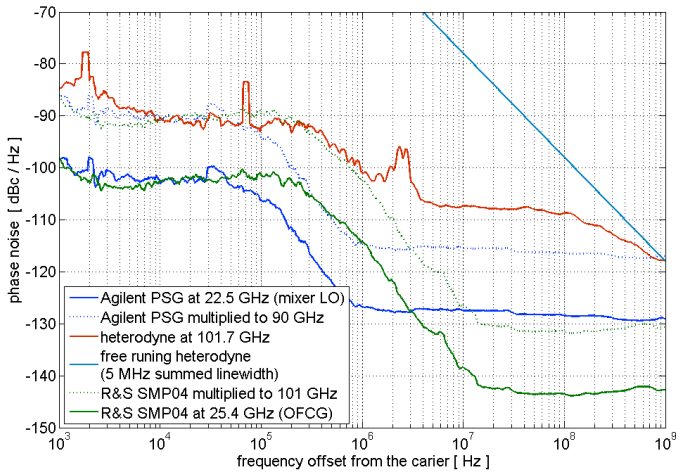

Fig. 7. Single-sideband phase noise of locked heterodyne signal at 101.7 GHz. The phase noise of the synthesisers used in the experiment are shown for comparison, as is the calculated phase noise for a free-running heterodyne with 5 MHz Lorentzian FWHM linewidth.

The phase noise spectra of the heterodyne signal were recorded using a Rhode & Schwarz FSU 26 GHz spectrum analyser set to phase noise measurement mode. The phase noise of the heterodyne signal was reduced to the level of less than -90 dBc/Hz at > 10 kHz offset. This level of noise is accounted for by the multiplied phase noise level of the synthesiser that was used to drive the phase modulator used for the optical comb generation.

The phase noise spectral densities of both synthesisers used in the experimental arrangement, together with expected phase noise of these signals after frequency multiplication [21], are included in Fig. 7 for reference. Due to the limited frequency range of the spectrum analyser used for phase noise measurements, the phase noise of the synthesiser used in the experiment was measured at the lower frequency of 22.5 GHz and scaled to

estimate the phase noise of 45 GHz LO and hence that of the 90 GHz LO within the SHM. This allowed to compare the phase noise of the synthesizer with the measured phase noise of heterodyne signal. It can be seen that the heterodyne signal phase noise at frequency offsets < 1 MHz is limited by the synthesisers used. Hence it could be anticipated that even higher spectral purity heterodyne signals could be generated by this PIC if synthesisers with lower phase noise had been used in the experiment.

The phase noise level of the 101.7 GHz heterodyne signal is below -108 dBc/Hz for frequency offsets from the carrier of 10 MHz or more. This phase noise suppression is due to the optical injection process and is determined by the slave laser linewidth and injection ratio. To achieve an optimum power injection ratio, a variable attenuator was introduced into the system. The amount of injected power was changed within a 15 dB range, which was reflected in various phase noise power spectral density of the heterodyne signal, as shown in Fig. 8.

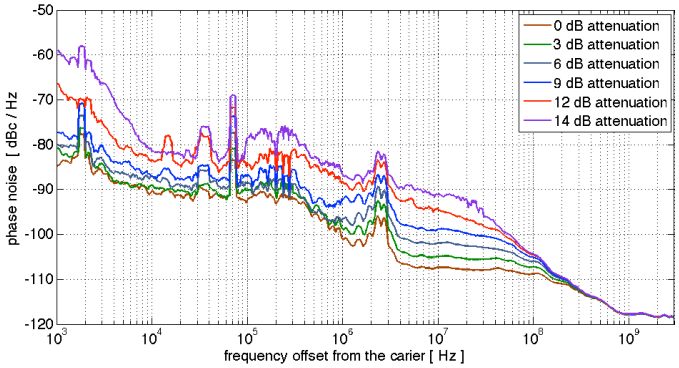

Fig. 8. SSB phase noise of locked heterodyne signal at different optical injection ratios

The measured power of down-converted mm-wave signal varied by less than 0.3 dB as the optical attenuation was changed by 14 dB. Such a small power change in the heterodyne signal level suggests that any excess phase noise in signals generated with higher attenuated injection is related to the optical injection process.

In principle, stable injection locking can be achieved if a small amount of power is injected into the SL cavity, as long as the difference between the frequencies of the free-running lasers remains within the locking range. For this PIC, the half locking range was measured to be between 250 MHz and 350 MHz (depending on the injected power level). Such a narrow locking range is determined by inversely proportional dependence of the laser cavity length [22] and hence is relatively small for these long (1.1 mm) DFB lasers. Moreover, the locking bandwidth remained dependent on the injected optical power, as well as the SOA1 current value. The long term stability of injection locking scheme remains dependent on temperature drift, which can cause change in the optical wavelength, and hence bring the device out of lock. This could be corrected by implementing optical injection phase lock loop [17].

In order to evaluate the output power performance of the PIC the sub-harmonic mixer was replaced by an Agilent E4418B power meter with the power sensor head W8486A, calibrated to measure the power of signals in the frequency range between 75 GHz and 110 GHz. In this measurement assembly the CPW coupled UTC-PD was probed using a coplanar probe connected to a suitable horn antenna. The probe has an incorporated bias tee, thus the UTC-PD could be biased at – 3 V and the generated DC photocurrent was measured. For the optimum operation point the total current used to drive the PIC was 389 mA (I_{DFB1} = 101 mA, I_{DFB1_PS} = 100 mA, I_{SOA2} = 90 mA, I_{SOA3}= 49 mA, I_{SOA4} = 49 mA) for a power consumption of about 800 mW, while the Peltier cooler was using 90 mW of electrical power, giving a total power consumption for the system of less than 1W. The free space transmission and connectors losses were estimated to be 2 dB. Correcting these losses signal of up to -10 dBm (-12 dBm reading) at 96 GHz for a 7.3 mA DC current in the UTC-PD was detected by the

power meter sensor head. During this measurement the PIC's optical output was constantly monitored on the optical spectrum analyser to confirm single mode operation of both DFB lasers. Moreover, the RF spectrum was also checked demonstrating a single peak at the desired frequency.

5. Conclusion

A monolithically integrated photonic source for mm-wave signal generation has been successfully demonstrated. Two semiconductor lasers were monolithically integrated on InP-based substrate together with numerous active and passive components, including two broad bandwidth photodiodes used to convert the optical heterodyne into a mm-wave signal. Maximum performance from the device was measured to be -10 dBm output power at 96 GHz for less than 1W of electrical power consumed. High-spectral-purity signals have been achieved by optically injection locking the two DFB lasers to a common reference optical frequency comb. Phase noise spectral density of a 101.7 GHz signal was measured to be less than -90 dBc/Hz for offsets from the carrier above 10 kHz. The spectral purity of the heterodyne signal could be further improved at low frequency offset (< 1 MHz) by employing a lower phase noise synthesizer for optical comb generation, and at larger frequency offset by reducing the linewidth of the integrated DFB lasers and optimising the optical injection locking conditions. Compact and tuneable sources with such characteristics offer some promising prospects for use as a mm-wave source in future communication networks.

Acknowledgements

This work was supported by the European Commission and carried out within the framework of the European STREP project iPHOS (www.iphos-project.eu) under Grant agreement no. 257539.